The Astrophysical Journal Letters, 819:L18 (7pp), 2016 March 10 doi:10.3847/2041-8205/819/2/L18

SOLAR JET–CORONAL HOLE COLLISION AND A CLOSELY RELATED CORONAL MASS EJECTION

Ruisheng Zheng, Yao Chen, Guohui Du, and Chuanyang Li
Shandong Provincial Key Laboratory of Optical Astronomy and Solar-Terrestrial Environment, and Institute of Space Sciences, Shandong University, 264209, Weihai, China; ruishengzheng@sdu.edu.cn
Received 2015 November 3; accepted 2016 February 15; published 2016 March 2

ABSTRACT

Jets are defined as impulsive, well-collimated upflows, occurring in different layers of the solar atmosphere with different scales. Their relationship with coronal mass ejections (CMEs), another type of solar impulsive events, remains elusive. Using high-quality imaging data from the Atmospheric Imaging Assembly/*Solar Dynamics Observatory*, we show a well-observed coronal jet event, in which the part of the jet with embedding coronal loops runs into a nearby coronal hole (CH) and gets bounced in the opposite direction. This is evidenced by the flat shape of the jet front during its interaction with the CH and the V-shaped feature in the time-slice plot of the interaction region. About a half-hour later, a CME with an initially narrow and jet-like front is observed by the LASCO C2 coronagraph propagating along the direction of the post-collision jet. We also observe some 304 Å dark material flowing from the jet–CH interaction region toward the CME. We thus suggest that the jet and the CME are physically connected, with the jet–CH collision and the large-scale magnetic topology of the CH being important in defining the eventual propagating direction of this particular jet–CME eruption.

Key words: Sun: activity – Sun: corona – Sun: coronal mass ejections (CMEs)

Supporting material: animations

1. INTRODUCTION

Solar coronal jets, first observed in X-rays with the Soft X-ray Telescope (XRT; Tsuneta et al. 1991) on board the *Yohkoh* satellite, represent a group of impulsive events characterized by well-collimated upflows with different scales developing in different layers of the solar atmosphere (e.g., Shibata et al. 1992; Savcheva et al. 2007; Chen et al. 2012). They are generally believed to be energized by magnetic reconnection, often associated with an inverse Y-shaped, anemone-like configuration involving open field lines in coronal holes (CHs) or open-like large-scale closed loops extending from an active region (Shibata et al. 1992, 2007; Schmieder et al. 1995; Pariat et al. 2009, 2015; Rachmeler et al. 2010). These open or open-like field lines are important in collimating jets.

Coronal mass ejections (CMEs) are another type of impulsive energy release event in the solar atmosphere, with a much larger scale and a stronger impact on nearby coronal structures such as streamers and CHs. There exist a number of studies examining the strong CME disturbance on coronal streamers (e.g., Hundhausen et al. 1987; Sheeley et al. 2000; Tripathi & Raouafi 2007; Chen et al. 2010). In the meantime, both streamers and CHs have been suggested to have effects on the propagating direction of CMEs, a crucial factor determining the CME geo-effectiveness. For instance, Gopalswamy et al. (2009) reported events with sources very close to the solar disk center that are unexpectedly *not* associated with interplanetary CMEs (yet accompanied by interplanetary shocks), and they attributed this to possible interaction and further deflection of CMEs by nearby CH(s). Nevertheless, a direct observation of this CME–CH interaction process remains absent. Nor do we know how and where the deflection takes place.

While both the jet and CME represent an impulsive ejection of plasma to upper levels of the solar atmosphere, their relationship remains obscure. Can a relatively large and fast jet drive a CME, or can the CME actually trigger some jets by, for example, opening an initially closed magnetic field? Different scenarios have been developed (e.g., Pariat et al. 2009, 2015), and actual answers may differ in different events, depending on specific circumstances.[1] It is also very interesting to ask, considering the above-mentioned possibility of a strong CME–CH interaction, can a jet, if moving along large-scale active region loops, actually interact with a nearby CH? This kind of event has never been reported. In this study, we present unambiguous evidence of such an event, revealing the collision between a set of coronal jets and a nearby CH with high-quality data from the Atmospheric Imaging Assembly (AIA; Lemen et al. 2012) on board the *Solar Dynamics Observatory* (*SDO*; Pesnell et al. 2012). It turns out that part of the jet is reflected toward the opposite direction, and this dynamical jet–CH interaction may have led to a successful eruption along the same direction.

2. OBSERVATIONS AND DATA ANALYSIS

We mainly analyzed the AIA/*SDO* data, which provides the essential observations of the event. The AIA instrument has 10 EUV and UV wavelengths, covering a wide range of temperatures. The AIA observes the full disk (4096×4096 pixels) of the Sun and up to 0.5 $R_{\odot}$ above the limb, with a pixel resolution of 0.″6 and a cadence of 12 s. The eruption is visible in all AIA EUV channels. The passbands of interest here are 131 Å (Fe XXI, ~10 MK), 211 Å (Fe XIV, ~2.0 MK), 171 Å (Fe IX, ~0.6 MK), and 304 Å (He II, ~0.05 MK). Magnetograms and intensity maps from the Helioseismic and Magnetic Imager (HMI; Scherrer et al. 2012), with a cadence of 45 s and pixel scale of 0.″6, were used to check the magnetic field configuration of the source region. The CME evolution in the

[1] Note that during the peer-review process of our manuscript, a study reporting a CME event likely triggered by a coronal jet was published (Liu et al. 2015), which presents evidence supporting the close relation between a jet and a CME, with the jet pushing an overlying blob-like magnetic structure that later becomes the CME front, and the jet likely evolves into the CME core.

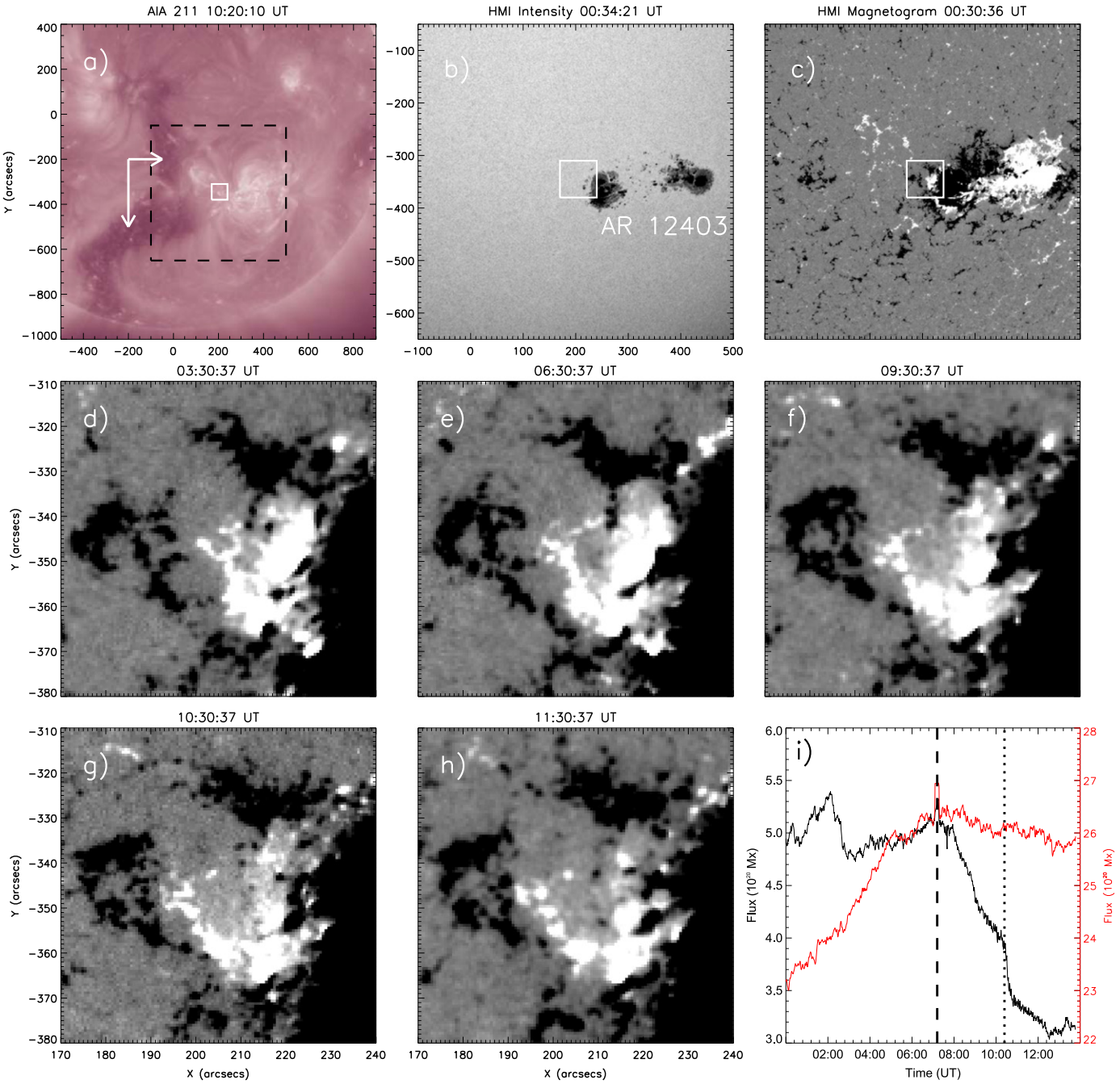

Figure 1. Overview of NOAA AR 12043 and the magnetic evolution of the event. (a) AIA 211 Å image showing the eruption region (white box) and the adjacent "elephant trunk" CH (white arrows), in which the black box indicates the FOV of (b)–(c). (b)–(c) HMI intensity map and HMI magnetogram showing the eruption region (white box) and the AR. (d)–(h) A sequence of HMI magnetograms showing the magnetic cancellation regions in an FOV indicated by the box in panel (c). (i) The changes in the negative (red) and positive (black) magnetic fluxes within the FOV of panels (d)–(h). The vertical dashed and dotted lines mark the onset of the abrupt decreasing and beginning of the eruption, respectively.

high corona was captured by the Large Angle and Spectrometric Coronagraph (LASCO) C2 (Brueckner et al. 1995).

The kinematics of the jets and associated mass flow were analyzed using the time-slice approach. The speeds were determined by linear fits, with error bars given by the measurement uncertainty, which is assumed to be 4 pixels (~1.74 Mm) for AIA data. We also used the Potential Field Source Surface (PFSS; Schrijver & De Rosa 2003) model to extrapolate the HMI photospheric field measurement to describe the large-scale magnetic field geometry.

3. RESULTS

3.1. Coronal Jets

The event occurred at the eastern boundary of the NOAA Active Region (AR) 12403 on 2015 August 25. The upper panels of Figure 1 show the AR image observed at AIA 211 Å and the intensity map and magnetogram of the HMI. The small white boxes (~S14E13) present the source area in which jets originated. It can be seen that the AR consists of a positive-polarity leading sunspot and a negative-polarity following

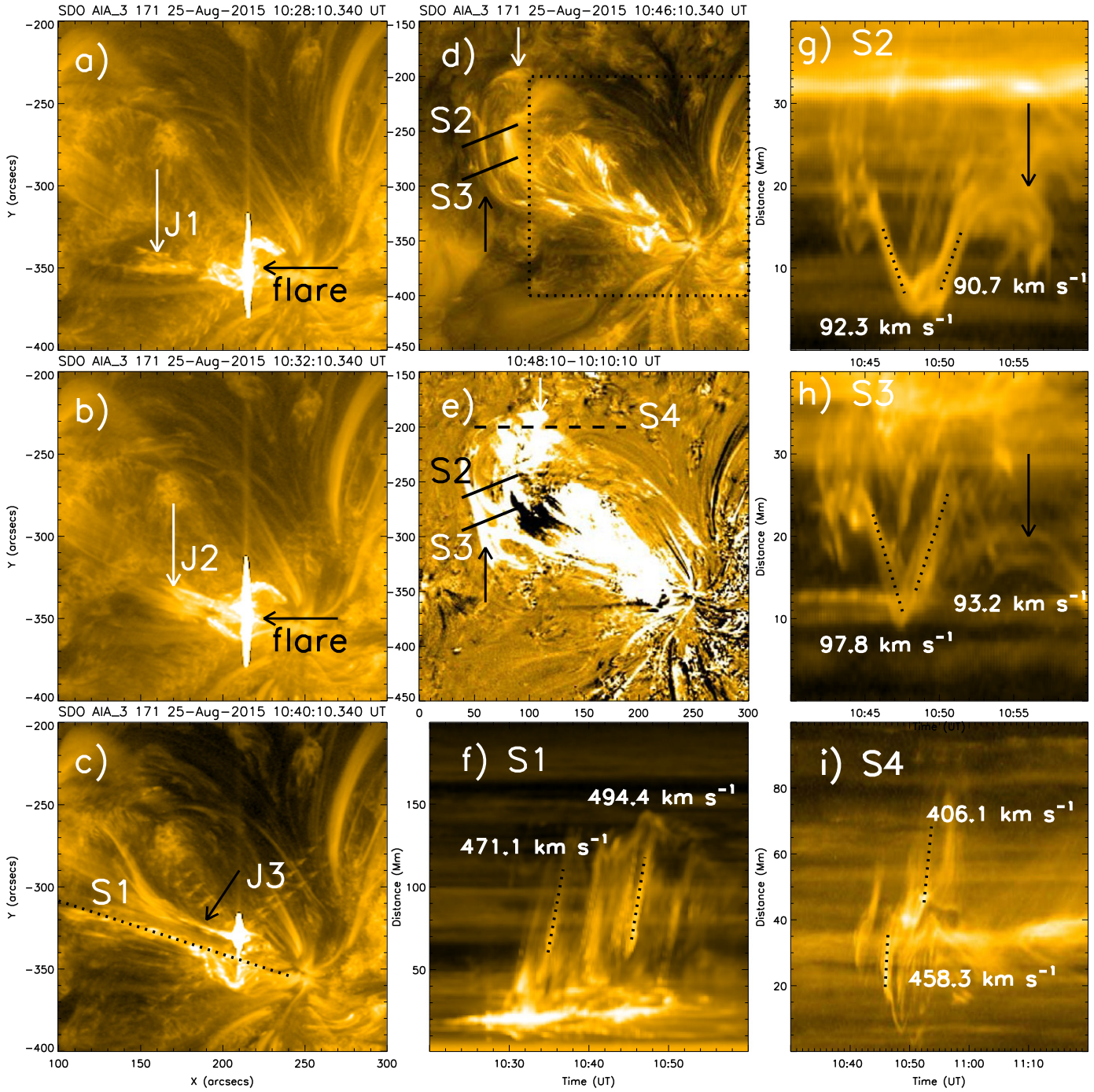

Figure 2. Coronal jets and their interaction with the nearby CH, observed at AIA 171 Å. (a)–(c) Images showing the coronal jets (J1–J3) and the associated flaring loops. (d)–(e) Images showing the jet–CH interaction. The short lines (S2–S3) are used to construct slice–time plots revealing the deflection of the jet-loop structure. The black dashed box in (d) indicates the FOV of (a)–(c). (f) Slice–time plot showing the motion of J2 along S1. (g)–(h) Slice–time plots along slices S2–S3. The flow stagnation is shown by black arrows. (i) Slice–time plot along S4. The dotted lines are used to derive the linearly fitted speeds.

(An animation of this figure is available.)

sunspot. In the region given by white boxes, there exists a small parasitic positive polarity. An elongated low-latitude elephant trunk CH exists eastward of the AR (white arrows in Figure 1(a)).

In Figures 1(d)–(h), we present the sequence of the HMI magnetogram from 03:30 UT to 11:30 UT to examine the magnetic evolution of the jet source region. As a result of earlier magnetic flux emergence, a small positive patch was embraced by negative dominant polarities and became the parasitic polarity. Comparing these magnetograms, we see that significant flux cancellation took place. This is further confirmed by the temporal changes of positive and negative magnetic fluxes in the field of view (FOV) of Figures 1(d)–(h), as plotted in Figure 1(i). Before 07:12 UT (dashed vertical line), the negative flux increased continuously, while the positive counterpart did not change much. After 07:12 UT,

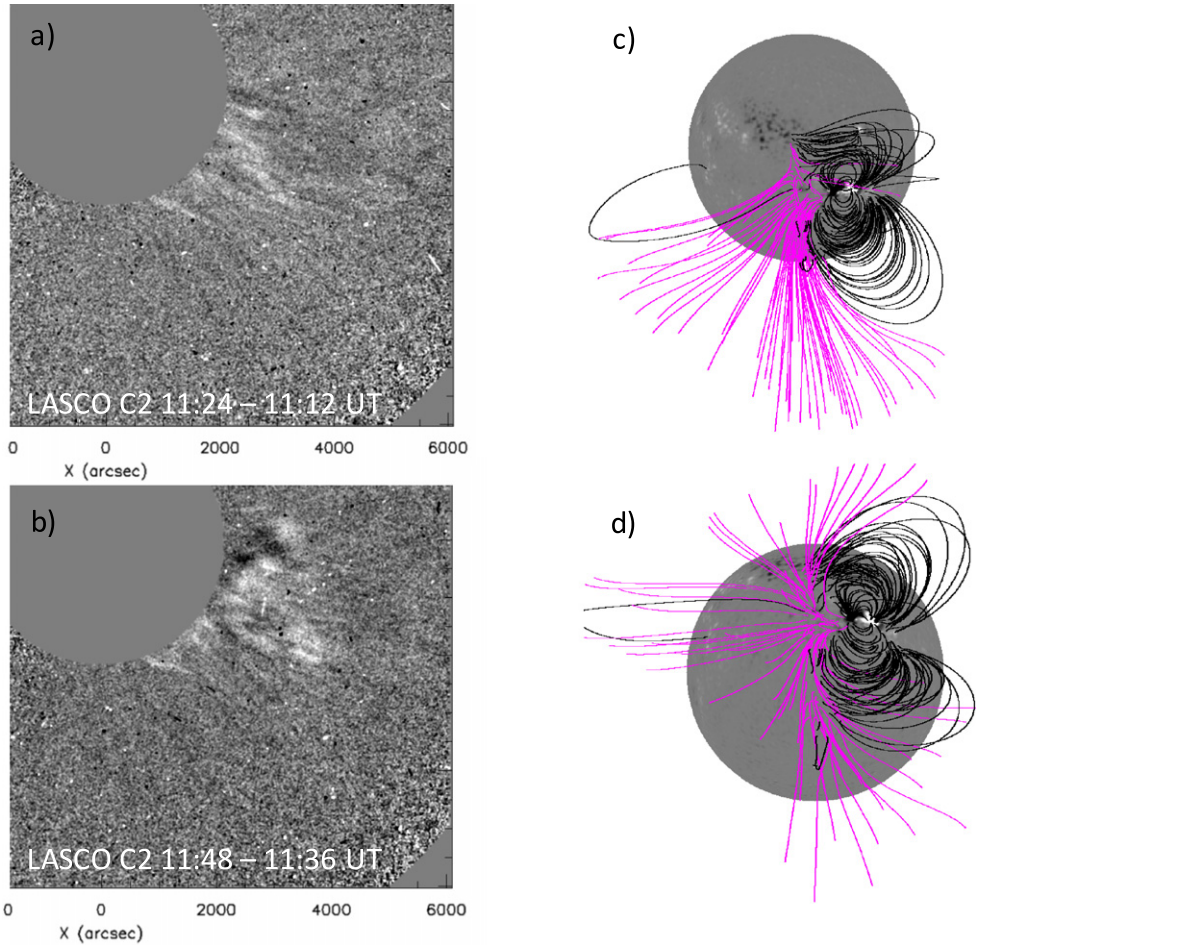

Figure 3. CME evolution and PFSS extrapolation results. (a)–(b) LASCO C2 images of the CME. (c)–(d) PFSS extrapolated field lines for the CH open field lines (purple) and the active region closed field lines (black). Panel (c) corresponds to the AIA FOV, while panel (d) is given by an upward (northward) rotation of panel (c) by 50° to show more details of the over expansion of the CH magnetic field lines.

(An animation of this figure is available.)

both fluxes started to decrease, with the positive one changing at a much steeper gradient. At about 10:20 UT (dotted vertical line), the positive flux presented an even faster declining rate.

The later time was consistent with the onset of the jet event. In the meantime, the GOES soft X-ray (SXR) profiles started to increase after 10:23 UT. Two SXR peaks were recorded in the following hour, corresponding to a C1.7 flare (peaking at 10:34 UT) and a C2.2 flare (peaking at 10:44 UT), respectively. Both flares were associated with jet activities. This is consistent with the general picture that jets are energized by magnetic reconnection, as evidenced here by significant flux cancellation and flare occurrence (e.g., Wang et al. 1998; Chae et al. 1999; Chifor et al. 2008; Pariat et al. 2009, 2015; Liu et al. 2011; Yang et al. 2011).

In Figure 2, we present the dynamical evolution of coronal jets observed at AIA 171 Å. As seen from Figures 2(a)–(c) and the accompanying animation, the jet started from the southern end of the bright flaring loops, exhibiting a gradual footpoint migration toward the northern end. The migration indicates an apparent motion of the main flaring reconnection site. For convenience of description, we separate the jets into three subsequent episodes, consisting of the initial relatively weak part (J1, starting at 10:26 UT), the middle part, which is the strongest one and of particular interest to this study (J2, starting at 10:30 UT), and the third part, which is basically confined by underlying loops (J3, starting at 10:38 UT). Note that similar confining mass flows have been used to trace the twisted internal structure of a flux rope (e.g., Li & Zhang 2013; Yang et al. 2014). These episodes of jets have been pointed out in Figures 2(a)–(c). As mentioned, the jets mainly emanated from the FOV of Figures 1(d)–(h), above the parasitic polarity. This is a general source property prescribed in jet modeling (e.g., Pariat et al. 2009, 2015). Because J1 was relatively weak and J3 was mostly confined, here we focus our study on J2.

Using the time-slice approach along the dotted line (S1) in Figure 2(c), the derived velocity of J2 is close to 500 km s^{-1} (Figure 2(f)), much faster than the statistical average speed of ~200 km s^{-1} for jets (Shimojo et al. 1996). It is clear that J2 lasted for ~30 minutes with continuous mass ejection. J2 initially moved along its associated AR loops, and extended the loops. It is interesting to see that the forward extension of the jet-loop structure was suddenly stopped. The curved side of the jet-loop structure became flat-shaped with kinks at both ends, and part of J2 was clearly bounced in the opposite direction while the left part returned to the solar surface (best seen in the animation). The first sign of bounced-back material was present around 10:38 UT as seen from the animation. The flat-shaped feature appeared around the interface between the nearby CH

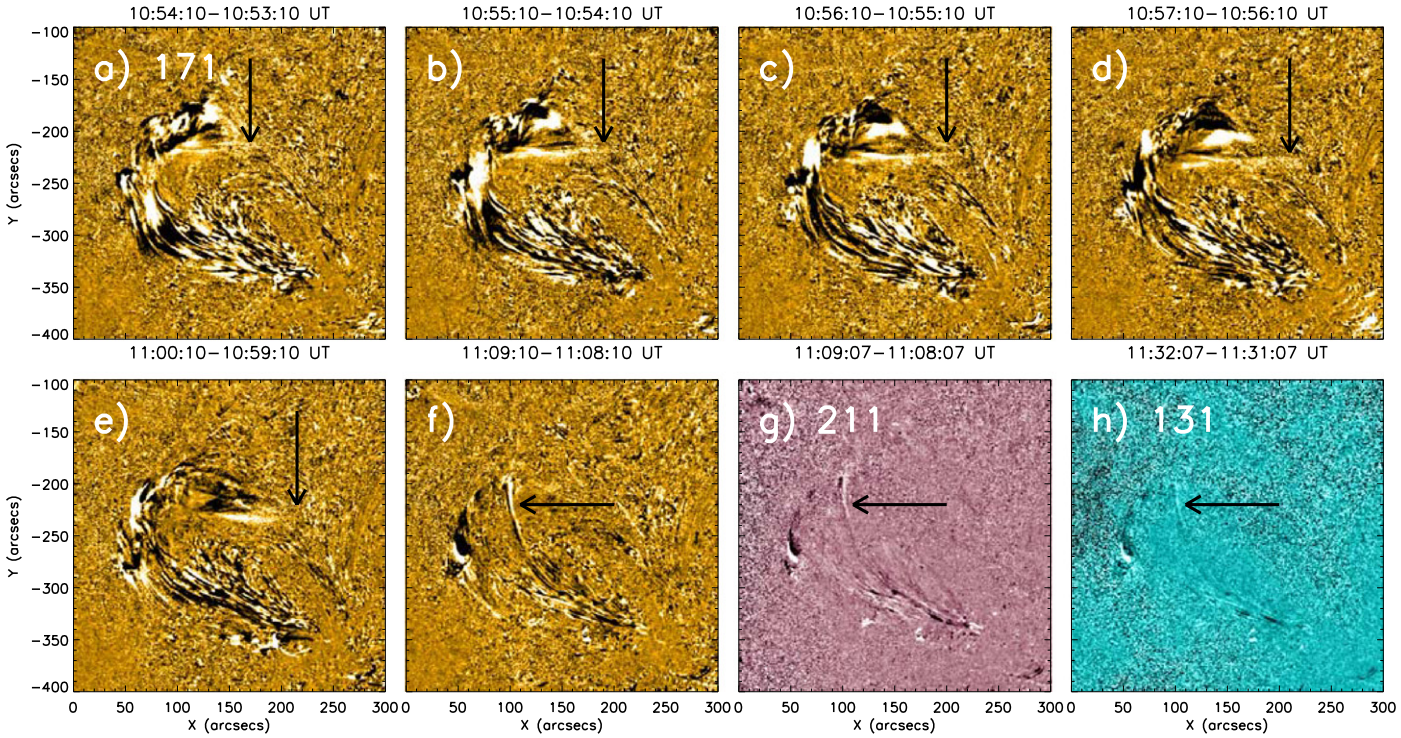

Figure 4. AIA images at 171 (a)–(d), 211 (e)–(f), and 131 Å (g)–(h) highlighting the continuation of the jet mass flow toward the west and the associated post-jet motion. Arrows in (a)–(d) point to the fast westward-moving jet fronts, and arrows in (e)–(h) point to the relatively slow westward-moving loops.
(Animations (a, b, and c) of this figure are available.)

and the east edge of the AR, indicating that the jet carrying the loop ran into the AR–CH boundary and got reflected there. The reflection is also seen from the height–time plot along slices S2 and S3 (short lines in Figures 2(d)–(e)), from which we see a distinct V-type structure (Figures 2(g)–(h)). The speeds of the jet-loop structure along S2 and S3 before and after the reflection are nearly the same (~90 km s^{-1}).

Note that after the jet–CH interaction, part of the jet material stagnated (black arrows in Figures 2(g)–(h)) while the left part presented a signature of continuation of mass flows toward the west (white arrows in Figures 2(d)–(e); see also the animation) at a fast speed of ~400 km s^{-1}. See Figure 2(i) for the time-slice plot along S4. This is only slightly slower than the pre-collision jet. Yet the jet front faded away shortly, so it is not known, at this time, whether the reflected jet flows have escaped the corona or not.

3.2. The CME and Its Relation with the Jet

A weak CME feature appeared in the LASCO C2 FOV at 11:14 UT, with a hardly identifiable narrow front, developing into a much clearer CME structure in 10–20 minutes (see Figure 3 and the accompanying animation). The central position angle of the ejecta at 11:26 UT was 238° (the angle increases counterclockwise with 0° along the north). Initially the CME presented a narrow jet-like morphology and later became diffusive without a clear flux-rope signature. It is thus difficult to determine the exact type of this eruption (see Vourlidas et al. 2013). The appearance time of a clear CME signature in C2 is about 50 minutes later than the first sign of the jet–CH collision (~10:38 UT). In addition, the continuation part of the reflected jet flow is basically toward the CME direction. This close temporal–spatial correlation suggests that the jet may be associated with the CME.

It is crucial to further figure out whether the jet front continued its westward motion toward the solar limb to become a part of the CME or if it actually moved downward along a curved loop path and was confined there. For short, we refer to these suggestions as the eruptive picture and the confining picture, respectively. In the following we present observational facts that, from our point of view, favor the first possibility.

First, from Figure 4 and its accompanying animations, in which a set of AIA images at 171, 211, and 131 Å are presented, we see that after 10:55 UT the jet front seemed to have moved beyond the associated AR loop system before its eventual fading away, as shown by the arrows in Figures 4(a)–(e), rather than returning to the solar surface along a curved loop-like path if it was confined.

Second, following the jet front, since 11:06 UT a systematic westward motion of a set of loops started to appear, as shown by arrows in Figures 4(f)–(h), with a speed of 10–20 km s^{-1}. This is best seen from the animations. The motion lasted for more than 30 minutes, possibly an effect of continuous stretching exerted by the westward mass motion. Again, this is not inconsistent with the eruptive picture.

Third, from the 304 Å data we observed an obvious outflow of filament-like dark material after 11:20 UT (see the white box in Figures 5(a)–(c)). It seems that the material corresponded to part of the reflected jet, being stagnated and accumulated around the jet–CH interaction region (best seen from the accompanying animation). They became dark possibly due to a cooling process. Note that there was no filament eruption observed during the event, so the dark material was not due to any filament eruption. Its outflow speed (~239 km s^{-1}) can be

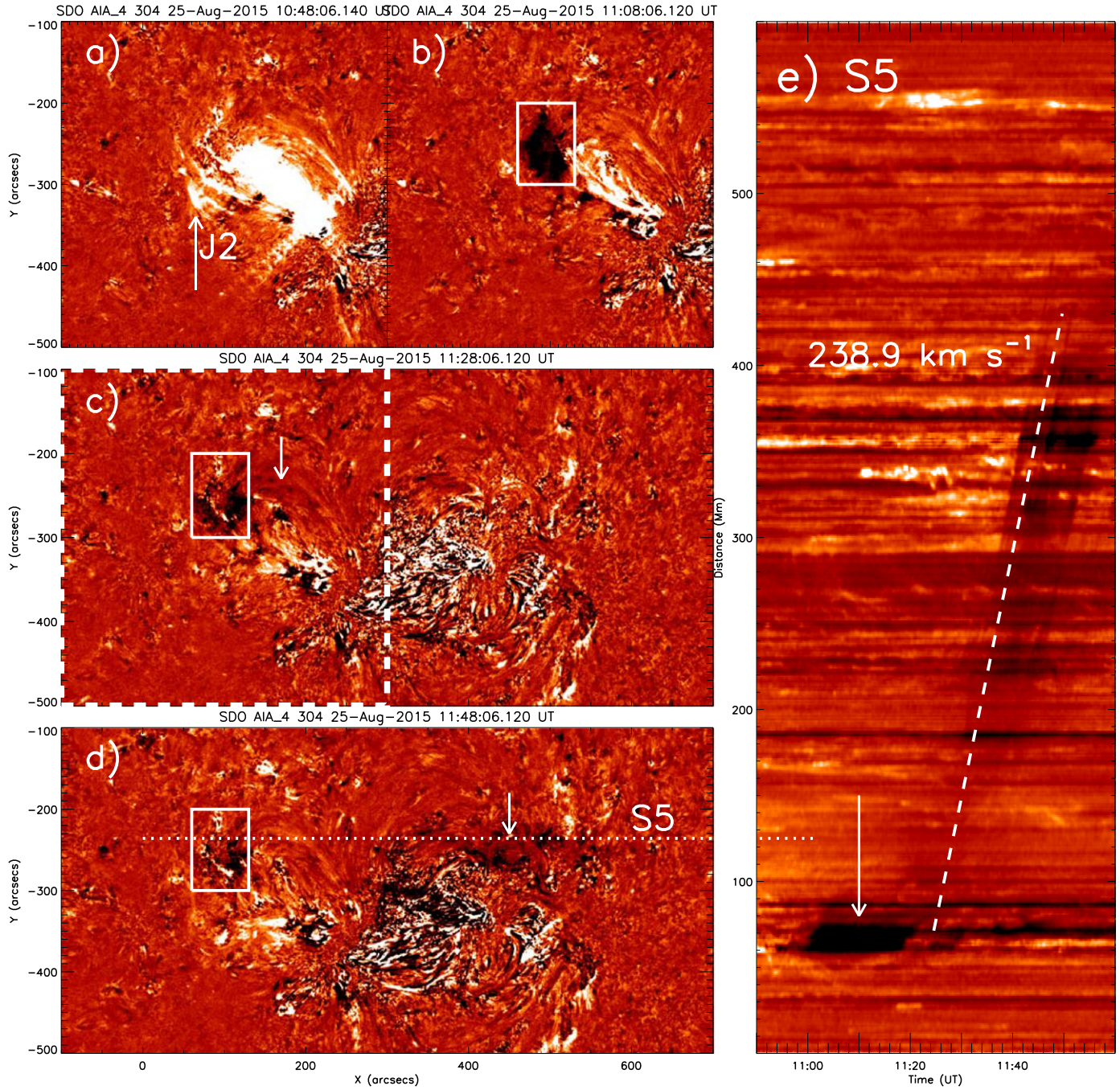

Figure 5. Accumulation and drift of the dark filament-like mass observed at AIA 304 Å. (a)–(b) Base-difference images exhibiting the accumulation of the jet mass as indicated by the white box. (c)–(d) Base-difference images illustrating the drift of the 304 Å material (white arrows). The dotted line in panel (d) is selected to construct a slice–time plot displaying the mass flow. The dashed box in panel (c) indicates the FOV of panels (a)–(b). (e) Slice–time plot along the slice S5. The dashed line is used to obtain the speed of the mass flow.

(An animation of this figure is available.)

derived using the distance–time analysis along the slice S5 (Figure 5(d)). The 304 Å material moved out of the AR along the direction pointing to the CME. This traces the open path from the jet–CH collision region to the CME, providing additional support for the first picture. Note that due to the time delay, the 304 Å material could not become the CME front, yet it may provide some mass to the eruption.

The last observational fact worthy of mentioning is that no other detectable eruptive activities were present on the solar disk according to all passband data of AIA, or on the back side according to the Extreme Ultraviolet Imager (EUVI; Howard et al. 2008) on board the twin spacecraft of the *Solar-Terrestrial Relations Observatory* (*STEREO*; Kaiser et al. 2008) with separation angles from the Earth of 172°.348 (*STEREO-A*) and 175°.495 (*STEREO-B*) at the time.

In summary, the above observational facts favor the first picture, i.e., the post-collision jet further evolves into part of the CME. The distance from the jet–CH interaction region to the

CME front is $\sim 3\,R_{\odot}$, indicating an average projected propagation speed of $\sim 700\,\mathrm{km\,s^{-1}}$ if assuming the post-collision jet front later becomes the CME front. This is faster than the AIA-measured projection speed of the jet, suggesting that either the jet gets further accelerated during its outward propagation or the jet is not the counterpart of the CME front and there exist other or earlier eruptive magnetic structures ahead of the jet. It should be pointed out that how the jet evolves into the CME and exactly which part of the CME corresponds to the jet front remains unresolved with the available data set, partly due to the absence of CME signatures in the AIA FOV.

Further examining the PFSS results of the CH–AR magnetic field lines (Figures 3(c)–(d)), we see that the CH open field lines are of negative polarity and lie next to the closed loop system that is rooted at the large negative polarity of the AR. The CH field lines, with strong non-radial expansion, occupy the space above the closed AR loops. This magnetic configuration helps us understand how the observed initially collimated jet (along the eastern edge of the AR) runs into field lines of the nearby CH and then flows outward along the specific trajectory.

4. SUMMARY

Here we present a first of its kind observational study on a jet–CH colliding process showing that the post-collision jet was reflected in the opposite direction. We also present compelling evidence supporting that the jet activity may have developed into a successful eruption (i.e., a CME). The jet–CH collision is evidenced by the flat morphology of the jet front observed by AIA, while the jet–CME relation is supported by their close temporal–spatial correlation, the observed outflow at 304 Å, the large-scale CH–AR magnetic field configuration given by PFSS, and the fact that there are no other identifiable eruptive activities on the solar surface including the backside, among other observations. The presumed jet–CME route basically follows the over-expanding trend of the CH open field lines above the AR according to PFSS extrapolation, indicating a strong role played by the CH structure in defining the CME propagation direction. This is consistent with earlier studies, which were, however, not based on direct observation of CME–CH interaction, that CHs are important in affecting the CME propagating direction and thus the consequent geo-effectiveness. The study is possible because of the unprecedented high-quality data of AIA/*SDO*.

SDO is a mission of NASA's Living With a Star Program. The authors thank the *SDO* team for providing the data. This work is supported by grants NSBRSF 2012CB825601, NNSFC 41274175, and 41331068, and Yunnan Province Natural Science Foundation 2013FB085.

REFERENCES

Brueckner, G. E., Howard, R. A., Koomen, M. J., et al. 1995, SoPh, 162, 357
Chae, J., Qiu, J., Wang, H., & Goode, P. R. 1999, ApJ, 513, 75
Chen, H., Zhang, J., & Ma, S. 2012, RAA, 12, 573
Chen, Y., Song, H. Q., Li, B., et al. 2010, ApJ, 714, 644
Chifor, C., Isobe, H., Mason, H. E., et al. 2008, A&A, 491, 279
Gopalswamy, N., Mäkeä, P., Xie, H., Akiyama, S., & Yashiro, S. 2009, JGRA, 114, A00A22
Howard, R. A., Moses, J. D., Vourlidas, A., et al. 2008, SSRv, 136, 67
Hundhausen, A. J., Holzer, T. E., & Low, B. C. 1987, JGR, 92, 11173
Kaiser, M. L., Kucera, T. A., Davila, J. M., St., et al. 2008, SSRv, 136, 5
Lemen, J. R., Title, A. M., Akin, D. J., et al. 2012, SoPh, 275, 17
Li, T., & Zhang, J. 2013, ApJL, 770, L25
Liu, C., Deng, N., Liu, R., et al. 2011, ApJL, 735, L18
Liu, J., Wang, Y., Shen, C., et al. 2015, ApJ, 813, 115
Pariat, E., Antiochos, S. K., & DeVore, C. R. 2009, ApJ, 691, 61
Pariat, E., Dalmasse, K., DeVore, C. R., Antiochos, S. K., & Karpen, J. T. 2015, A&A, 573, 130
Pesnell, W. D., Thompson, B. J., Chamberlin, P. C., et al. 2012, SoPh, 275, 3
Rachmeler, L. A., Pariat, E., DeForest, C. E., Antiochos, S. K., & Török, T. 2010, ApJ, 715, 1556
Savcheva, A., Cirtain, J., Deluca, E. E., et al. 2007, PASJ, 59, 771
Scherrer, P. H., Schou, J., Bush, R. I., et al. 2012, SoPh, 275, 207
Schmieder, B., Shibata, K., van Driel-Gesztelyi, L., & Freeland, S. 1995, SoPh, 156, 245
Schrijver, C. J., & De Rosa, M. L. 2003, SoPh, 212, 165
Sheeley, N. R., Hakala, W. N., & Wang, Y.-M. 2000, JGR, 105, 5081
Shibata, K., Ishido, Y., Acton, L. W., et al. 1992, PASJ, 44, 173
Shibata, K., Nakamura, T., Matsumoto, T., et al. 2007, Sci, 318, 1591
Shimojo, M., Hashimoto, S., Shibata, K., et al. 1996, PASJ, 48, 123
Tripathi, D., & Raouafi, N.-E. 2007, A&A, 473, 951
Tsuneta, S., Acton, L., Bruner, M., et al. 1991, SoPh, 136, 37
Vourlidas, A., Lynch, B. J., Howard, R. A., & Li, Y. 2013, SoPh, 284, 179
Wang, H., Johannesson, A., Stage, M., Lee, C., & Zirin, H. 1998, SoPh, 178, 55
Yang, S., Zhang, J., Li, T., & Liu, Y. 2011, ApJL, 732, L7
Yang, S., Zhang, J., Liu, Z., & Xiang, Y. 2014, ApJL, 784, L36